

Waveguides with uniaxially patterned layers

Serge Luryi^a and Arsen V. Subashiev^{a,b}

Department of Electrical and Computer Engineering,
State University of New York at Stony Brook, Stony Brook, NY 11794-2350;

^bSt. Petersburg State Technical University, St. Petersburg, 19251, Russia

ABSTRACT

We present an effective approach to calculating the low-frequency part of the spectrum of uniaxially patterned periodic structures. In this approach we ignore to zeroth-order the Bragg scattering by crystalline planes but include local field effects in first order perturbation theory. Bragg reflections are shown to be important only near points of symmetry-induced spectral degeneracy, where they can be taken into account by the degenerate perturbation theory. We apply this approach to waveguiding by thin patterned slabs embedded in a homogeneous medium. This results in an effective medium approximation, similar to the Maxwell Garnet theory but modified for the local field corrections specific to 2D geometry. Slab spectra are well described by a single frequency-independent parameter, which we call the guiding power. Simple analytic formulae are presented for both TM and TE polarizations. Comparing these formulae with similar expressions for homogeneous uniaxial slabs of same thickness, we derive the principal values of the effective homogeneous permittivity that provides identical waveguiding. We also discuss the extinction of waves due to the Rayleigh-like scattering on lattice imperfections in the slab. The TE waves that are normally better confined are scattered out more efficiently, in part because of the higher scattering cross-section and in part because the better confinement leads to higher exposure of TE waves to lattice imperfections in the slab.

Keywords: photonic crystals, waveguiding, modal control

1. INTRODUCTION

Waveguiding of light in layered patterned structures, such as slabs of 2D photonic crystals (PC), has attracted much interest in view of potential photonic applications.¹⁻³ The studied 2D patterns include periodic lattices of deep etched air pores or "conjugate" lattices of high permittivity cylinders. Structures where the inclusions can be considered infinite along the cylinder axis, will be called the 2D photonic crystals (PC) whereas finite-thickness periodic structures (including arrays of spheres) will be referred to as PC slabs. Patterned slabs (not necessarily periodic) can be employed as the waveguide core or cladding.

Numerous theoretical computations of the band spectra of 2D PC and PC slabs have been reported, based of expansions of the electromagnetic field in plane waves^{3,4} or cylindrical waves,^{5,6} as well as using finite-difference time-domain methods.^{7,8}

The low frequency region of the electromagnetic waves in the 2D PC is well understood. The waves have a linear spectrum that is very close to that obtained in the effective media approximation^{9,10} with an effective permittivity corresponding to the Maxwell Garnett theory.^{9,11} Thus, for the wavelength λ exceeding the structure period a , the optical properties are predominantly dependent only on the filling factor f of the inclusions (i.e. their fraction of the total volume), and do not rely on their long-range order or their shape variation (Sect. 2). The disorder leads to a weak (for $\lambda \gg a$) Rayleigh-like scattering.

Even though the effective media approach has been found to give excellent results up to very large permittivity contrast values of the pattern and for arbitrary propagation directions,¹¹ the question of how wide is its region of applicability and how close it can approach the Brillouin zone boundary has not been conclusively addressed, to our knowledge. The difficulty is apparently related to the poor convergence of the standard plane wave

Further author information:

SL: Phone (631) 632-8420, E-mail Serge.Luryi@stonybrook.edu,

AS: Phone (631) 632-8422, E-mail ASubashiev@ece.sunysb.edu

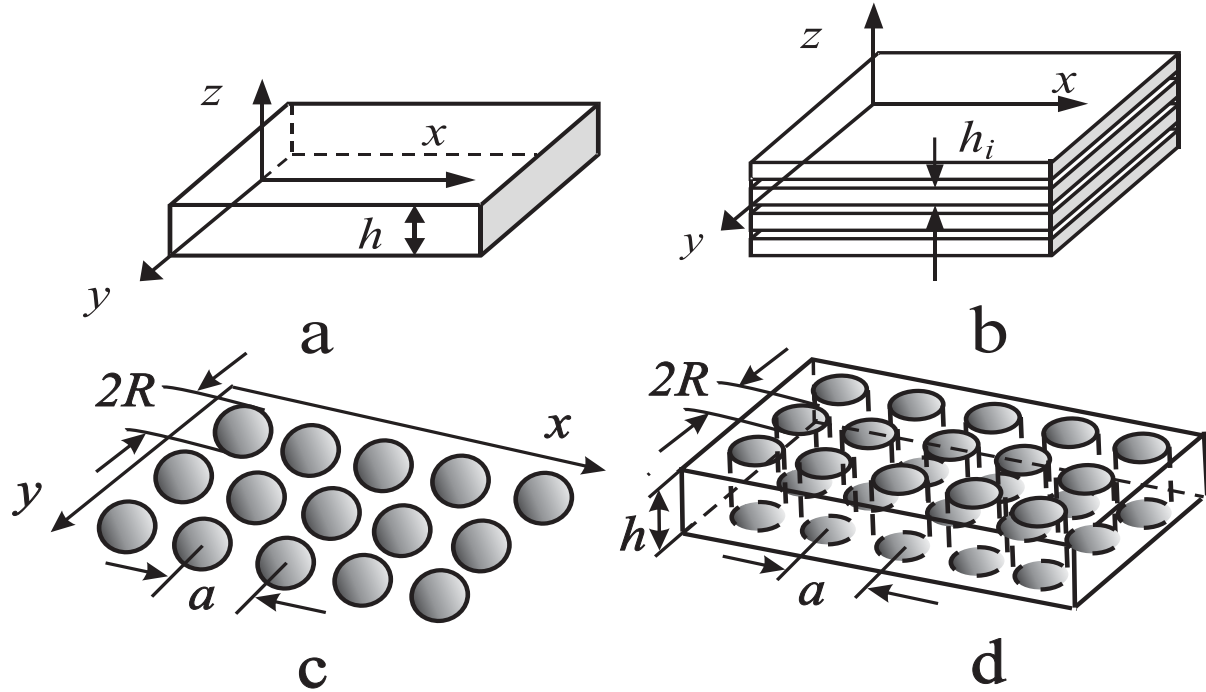


Figure 1. Slab waveguides considered in this work: (a) homogeneous three-layer waveguide with core of thickness h and permittivity ϵ_g embedded in a medium of background permittivity ϵ_b ; (b) multiple-layer core with $\epsilon = \epsilon(z)$; (c) monolayer array of spheres of radius R and period a ; (d) periodic array of cylinders (rods or pores) of height h , radius R and separation a . We also consider 2D photonic crystals, corresponding to (d) with $h \rightarrow \infty$

expansion with the increase of the included number of waves, especially for TM-like waves.⁶ Cylindrical waves offer a faster convergence, but still require the diagonalization of a 3×3 matrix, even in the quasi-static limit, in order to get the Maxwell Garnett result.^{5,11} This brings into question the accuracy of the effective medium approximation at frequencies where the linear spectrum can be strongly modified by the Bragg reflection. Here we shall demonstrate (Sect. 3) that with a proper choice of the zero-order waves the PC spectrum of the lowest branches can be calculated analytically all the way to the Brillouin zone boundary.

The waveguiding with PC slabs of thickness h relies on the average index guiding as modified by the periodic structure. We show that in the long wavelength limit the waveguiding remains effective even for structures with a low filling factor and weak index contrast, including highly inhomogeneous structures, $a \geq h$. Moreover, the waveguiding has a universal form described by a single parameter, which we shall call the "guiding power". It can be calculated by a self-consistent procedure for the polarizability of the dielectric pattern.

In Sect. 4 the guiding power is evaluated for several exemplary slab structures, illustrated in Fig. 1. As an extreme case, we discuss the waveguiding in highly inhomogeneous structures, such as planar regular arrangements of small (relative to their separation) dielectric spheres, nearly overlapping cylindrical pores or high-index cylindrical rods with large spacings. For thin slabs, the local field effects are different from those in an infinitely extended 2D PC, primarily because of the short-range dipolar interaction between the finite-height cylinders or spheres. Proper inclusion of the local field effects in the low-frequency region enables a perturbative approach with fast convergence.

The waveguiding with uniaxially patterned layers is strongly affected by their optical anisotropy. For a slab composed of high-index cylinders, the optical anisotropy can far exceed that of any natural crystal away from its absorption band. This anisotropy can be used to effect the modal control in practical photonic devices.¹²

Optical mode polarization is important for semiconductor lasers and amplifiers. It depends on the modal gain which in turn is controlled by both the gain anisotropy and the so-called modal confinement factor.^{13,14}

In a high-contrast three-layer waveguide the TE mode is better confined than the TM mode and therefore for an isotropic amplifying material the TE mode has a larger gain.^{15,16} However, in III-V heterostructures the index contrast between the core and cladding layers is small. The guiding power in such waveguides is weak, and patterning creates a modal competition due to the uniaxial anisotropy. As a result, the guiding power for the TM wave and the associated modal confinement and gain can exceed those for the TE wave. This type of modal competition was discussed in our earlier work¹² and is further discussed in Sect. 4.

Here we shall also discuss (Sect. 5) the effects of wave extinction due to the scattering on imperfections in a non-ideal slab. The extinction coefficient depends on the guiding power of the core and the polarizability of the inclusions, both of which are different for the two mode polarizations. When the imperfections are mainly in the core, one finds a paradoxical situation that the mode which is better confined becomes extinct faster. Moreover, cylindrical imperfections radiate the TE mode more efficiently. Both of these effects can shift the modal competition in favor of the TM mode.

2. WAVEGUIDING IN THE LATERALLY UNIFORM WAVEGUIDE APPROXIMATION

We begin with the well-known case of a laterally uniform three-layer dielectric waveguide (Fig. 1a) and introduce the concept of *guiding power* in terms of familiar parameters. Outside the slab the dispersion equation is of the form

$$\epsilon_b k_0^2 = q^2 - \kappa^2, \quad (1)$$

where $k_0 = \omega/c$ is the frequency parameter, ϵ_b is the background (cladding) permittivity and \mathbf{q} is the 2D wave vector in the plane of the waveguide. The parameter κ describing the exponential decay, $\exp(-\kappa z)$, of the wave away from the core, depends on frequency. It is convenient to introduce a frequency-independent parameter g

$$\kappa = \frac{1}{2} \epsilon_b k_0^2 g, \quad (2)$$

which we shall call the “guiding power” of the high-index core. Equation (2) with a constant g holds¹³ for a three-layer dielectric waveguide of core thickness h , provided $\kappa h \ll 1$. In this limit Eqs. (1, 2) define a universal dispersion relation for the guided modes.

If the guiding layer (core) permittivity is ϵ_g , the value of g for the two polarizations is given by

$$g_{\text{TE}} = \frac{\epsilon_g - \epsilon_b}{\epsilon_b} h, \quad g_{\text{TM}} = \frac{\epsilon_g - \epsilon_b}{\epsilon_g} h. \quad (3)$$

In structures with low index contrast, when $(\epsilon_g - \epsilon_b) \ll \epsilon_b$ the values of g for the two modes are small and close to each other. In the opposite limit, $(\epsilon_g/\epsilon_b) \gg 1$, the guiding power for the TM mode is ϵ_b/ϵ_g times weaker than g_{TE} , which can be explained by the reduced z component of the electric field inside the slab.

Confinement of guided waves is described by the dimensionless “confinement factor” $\Gamma = \kappa h$ (fraction of the wave intensity that flows in the high-index core). Quite generally, Γ is proportional to the guiding power. The condition $\Gamma \ll 1$ describes the *weak guiding limit*. In this limit Eqs. (1, 2) remain valid for an arbitrary laterally uniform multilayer waveguide with $\epsilon = \epsilon(z)$, Fig. 1b. The guiding power is then given by the following expressions (see Appendix):

$$g_{\text{TE}} = \int_{-\infty}^{\infty} \left(\frac{\epsilon(z)}{\epsilon_b} - 1 \right) dz, \quad g_{\text{TM}} = \int_{-\infty}^{\infty} \left(1 - \frac{\epsilon_b}{\epsilon(z)} \right) dz. \quad (4)$$

The guiding power remains the only parameter of the index profile that defines both the confinement properties and the dispersion of waves in the weak guiding limit.

We now turn to structures with a uniaxially patterned guiding layer, Figs. 1c,d. In the long wavelength limit ($\lambda \gg a$) such structures, though inhomogeneous, can be viewed in the effective medium approximation. The structure composed of cylinders, Fig. 1d, is optically uniaxial with the axis C directed perpendicular to the waveguide plane. We denote by ϵ_{\parallel} and ϵ_{\perp} the effective medium permittivities for the two possible electric field

orientations. For $\lambda \gg a$, these permittivities can be calculated using the Maxwell Garnett approximation, which neglects the depolarization effects associated with the finite height of the cylinders.

When the electric field $\mathbf{E} \parallel \mathbf{C}$, the effective permittivity coincides with that obtained by direct averaging, viz.

$$\epsilon_{\parallel} = \epsilon_{out} + (\epsilon_{in} - \epsilon_{out})f \quad (5)$$

Here ϵ_{in} and ϵ_{out} are the material permittivities inside and outside the cylinders, respectively.

When the electric field $\mathbf{E} \perp \mathbf{C}$, the effective permittivity is given by

$$\epsilon_{\perp} = \epsilon_{out} \frac{(\epsilon_{in} + \epsilon_{out}) + (\epsilon_{in} - \epsilon_{out})f}{(\epsilon_{in} + \epsilon_{out}) - (\epsilon_{in} - \epsilon_{out})f}. \quad (6)$$

The dependence of ϵ_{\parallel} and ϵ_{\perp} on the filling factor is depicted in Fig. 2 for cylindrical pores in a dielectric medium, taking $\epsilon_{in} = 1$ and $\epsilon_{out} = 12$. An appreciable anisotropy of the permittivity is evident. The figure also shows the effective permittivities for a “conjugate” crystal of cylinder rods in air, corresponding to the replacement $\epsilon_{out} \rightleftharpoons \epsilon_{in}$. This geometry gives higher optical anisotropy, especially for low filling factors.

Equations (5, 6) are derived for infinite cylinders and can be expected to fail when applied to optical properties of thin layers when the height of the cylinders is comparable to their diameter. This case is considered in Sect. 4, where we show that the effective media approach remains valid, but requires a modification of Eq. (6) allowing for the depolarization factors of the finite height cylinders.

For a sufficiently thick core layer $h \gg a$, the guided-wave spectra in the low frequency range $\sqrt{\epsilon}k_0 \leq \pi/a$ can be obtained by the usual approach^{13,14} developed for homogeneous waveguide constituents. We take into account the layer anisotropy¹² by treating the TE mode as an *ordinary* wave and the TM mode as an *extraordinary* wave, propagating in a uniaxial crystal. The crystalline pattern begins to affect the waveguiding only when the propagation wave vector approaches a narrow range near the Bragg reflection planes, $\mathbf{q} \approx \mathbf{G}/2$, where \mathbf{G} is one of the vectors of the 2D reciprocal lattice.¹⁷

3. LOW FREQUENCY PART OF PC SPECTRA

Before evaluating the guiding power of a PC slab, we test our approach by calculating the lowest-bands spectra of a 2D PC infinitely extended in the z direction. This calculation gives an effective index of the guiding layer regarded as an infinite PC. With its help we can expect to sort out all issues associated with Bragg reflection near the Brillouin zone boundary, but not the thin-slab depolarization effects to be considered in Sect.4.

TM mode

For the TM mode the electric field is along the cylinder axes and the wave equation

$$\Delta \mathbf{E} - \text{grad div} \mathbf{E} = -k_0^2 \epsilon(\mathbf{r}) \mathbf{E}, \quad (7)$$

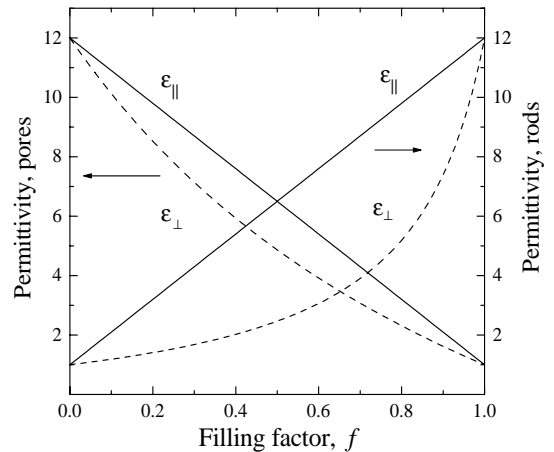


Figure 2. Average permittivity in a uniaxially patterned Si layer as a function of the filling factor f . We consider a planar lattice of cylindrical pores or rods with the axis of symmetry \mathbf{C} perpendicular to the plane of the lattice. Solid lines show ϵ_{\parallel} ($\mathbf{E} \parallel \mathbf{C}$) and dashed lines ϵ_{\perp} ($\mathbf{E} \perp \mathbf{C}$), plotted according to Eqs. (5, 6). For pores $\epsilon_{in} = 1$, $\epsilon_{out} = 12$ and for rods $\epsilon_{in} \rightleftharpoons \epsilon_{out}$.

is easily transformed into a matrix form by using the Fourier expansions of both the electric field and the dielectric function, taking into account the PC periodicity. The Fourier components of $\epsilon(\mathbf{r})$ are of the form⁴

$$\epsilon(\mathbf{G}) = \begin{cases} \epsilon_{out} + f(\epsilon_{in} - \epsilon_{out}), & \mathbf{G} = 0 \\ f(\epsilon_{in} - \epsilon_{out})2J_1(GR)/(GR), & \mathbf{G} \neq 0 \end{cases} \quad (8)$$

We consider the wave propagating in the plane perpendicular to the cylinder axes, $\mathbf{k} = \mathbf{q}$, $k_z = 0$. The Fourier coefficients $E_{\mathbf{q}}(\mathbf{G})$ of the electric field of this wave obey the following system of equations:

$$\left[\frac{(\mathbf{q} + \mathbf{G})^2}{\epsilon(0)} - k_0^2 \right] E_{\mathbf{q}}(\mathbf{G}) - \frac{k_0^2}{\epsilon(0)} \sum_{\mathbf{G}' \neq 0} \epsilon(\mathbf{G}') E_{\mathbf{q}}(\mathbf{G} + \mathbf{G}') = 0. \quad (9)$$

We see that in the long wavelength limit, when $k_0^2 \ll G^2/\epsilon(0)$ the main contribution to the mode comes from the term $E_{\mathbf{q}}(\mathbf{G})$ with $G = 0$, while higher-order corrections (originating from $E_{\mathbf{q}}(\mathbf{G})$ with $G \neq 0$) are proportional to an additional factor $k_0^2/[G^2\epsilon(0)] \ll 1$.

Thus, we find that in the long wavelength limit the dispersion relation is of the form $k_0 = q/\sqrt{\epsilon(0)}$. This means that the spectrum of electromagnetic waves is well described by the effective medium approximation with the average effective permittivity $\epsilon(0) = \epsilon_{out} + f(\epsilon_{in} - \epsilon_{out}) \equiv \epsilon_{\parallel}$.

The nondegenerate part of the lowest-band spectra can be calculated perturbatively, keeping the contributions of several nearest reciprocal lattice sites. The perturbation series corrections are given by

$$\frac{k_0^4}{\epsilon(0)} \sum_{\mathbf{G}'} \frac{\epsilon(\mathbf{G}')^2}{(\mathbf{q} + \mathbf{G}')^2/\epsilon(0) - k_0^2}, \quad (10)$$

so that in the low frequency region [$k_0^2 \leq G^2/\epsilon(0)$] the series converges rapidly due to the fast decrease of its terms with increasing \mathbf{G} .

However, this perturbative approach works well only away from the points of symmetry-induced spectral degeneracy, such as those at the Brillouin zone boundary. In the vicinity of these points, the spectrum is partially split and the splitting is of the first order in both $\epsilon(\mathbf{G})$ and k_0^2 . At multiply degenerate points the splitting has an additional large numerical factor. Still, the corrections remain relatively small below the first upper branch of the spectrum at Γ point.

The spectra calculated analytically for infinitely long cylindrical pores (cf. Fig. 1d) with $f = 0.385$ and $\epsilon_{out} = 12$ are shown in Fig. 3 and compared with a numerical calculation. The good agreement is not accidental. It reflects the rapid convergence of the perturbation series. For example, near the X point boundary of the square lattice the calculated corrections to the the first-order split frequencies, $k_0 = G/[2\sqrt{\epsilon_{\parallel} \pm \epsilon(G)}]$, $G = 2\pi/a$, are within $\pm 3\%$ for a wide range of the filling factor variation and different permittivity ratios.

The entire lowest branch of the spectrum can be obtained by truncating the system of equations. To obtain an accurate account of the splitting of degenerate zero-order waves, we need to include only the nearest sites of the reciprocal lattice with equal values of \mathbf{G} . For the second branch along ΓX or ΓM line in a square lattice we must consider a system of seven sites. To have a consistent description along the whole set of ΓX , ΓM and XM lines we have to include the contributions from 9 sites.

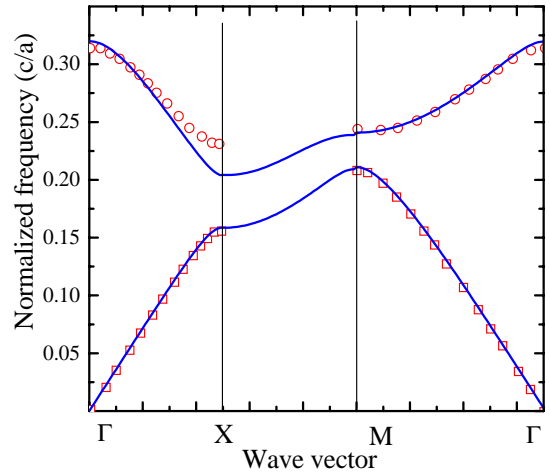


Figure 3. Low frequency spectra (TM polarization) of a photonic crystal (square lattice of cylindrical pores) calculated by the degenerate-state perturbation theory (solid lines). Results are compared with a numerical calculation²⁰ (points). Pore radius is $0.35a$ and the material permittivity is $\epsilon_{out} = 12$.

TE mode

For the TE mode ($\mathbf{E} \perp \mathbf{C}$) it is more convenient to recast the wave equation as an equation for the polarization vector of a cylinder.²¹ We begin with Eq. (7) written in the form

$$\Delta \mathbf{E} - \text{grad div} \mathbf{E} = -k_0^2 \mathbf{D}, \quad (11)$$

where \mathbf{D} is the displacement vector, $\mathbf{D} = \mathbf{E} + 4\pi \mathbf{P}$, and \mathbf{P} the polarization vector of the medium. For the sake of brevity, we shall proceed with the derivation assuming $\epsilon_b \equiv \epsilon_{out} = 1$ and in the final expression replace ϵ_{in} by $\epsilon_{in}/\epsilon_{out}$.

Next, we rewrite Eq. (11) in the form of an integral equation

$$E_\alpha = 4\pi k_0^2 \int d^3r G_{\alpha\beta}(\mathbf{r} - \mathbf{r}') P_\beta(\mathbf{r}'). \quad (12)$$

where $\alpha, \beta = x, y, z$, and $G_{\alpha\beta}(\mathbf{r} - \mathbf{r}')$ is Green's function defined by^{6, 22}

$$G_{\alpha\beta}(\mathbf{r} - \mathbf{r}') = \left(\delta_{\alpha\beta} + \frac{1}{k_0^2} \nabla_\alpha \nabla_\beta \right) G(\mathbf{r} - \mathbf{r}'), \quad (13)$$

where $G(\mathbf{r} - \mathbf{r}')$ is Green's function of the scalar Helmholtz equation

$$G(\mathbf{r} - \mathbf{r}') = \int \frac{d^3k}{(2\pi)^3} \frac{\exp[i\mathbf{k}(\mathbf{r} - \mathbf{r}')] }{k^2 - k_0^2}. \quad (14)$$

We seek the low-frequency wave-like solutions of Eq. (12) in the dipole approximation for the cylinder response to an external field. The field inside a cylinder in a smooth external field remains homogeneous.²³ For a set of non-overlapping cylinders we have

$$\mathbf{P}(\mathbf{r}) = \sum_{\mathbf{l}} \mathbf{P}_{\mathbf{l}}(\mathbf{r}), \quad \mathbf{P}_{\mathbf{l}}(\mathbf{r}) = \frac{\alpha_0}{v_0} \theta(\mathbf{r} - \mathbf{l}) \mathbf{E}(\mathbf{r}), \quad (15)$$

where \mathbf{l} are the lattice translation vectors, α_\perp is the cylinder polarizability

$$\alpha_\perp = \frac{1}{2} h R^2 \frac{\epsilon_{in} - 1}{\epsilon_{in} + 1}, \quad (16)$$

$v_0 = \pi R^2 h$ is the cylinder volume, R its radius, and $\theta(\mathbf{r})$ is the form-factor (a step-function that equals unity inside the cylinder and zero outside). For Bloch waves the spatial variation of polarization must be of the form

$$\mathbf{P}(\mathbf{r}) = \frac{\alpha_\perp}{v_0} \mathbf{E}_{\mathbf{q}} \exp(i\mathbf{q}\mathbf{r}) \sum_{\mathbf{l}} \theta(\mathbf{r} - \mathbf{l}) \exp(i\mathbf{q}(\mathbf{r} - \mathbf{l})) \quad (17)$$

Equation (12) can be used to calculate the electric field in a propagating wave excited by all the cylinders except one. Let the latter be the cylinder at $\mathbf{r} = \mathbf{l}$. We can calculate the dipole moment of this cylinder by including the electric field at $\mathbf{r} = \mathbf{l}$ produced by all other cylinders and multiplied by $\alpha_\perp \theta(\mathbf{r} - \mathbf{l})$. In this way we avoid the problem of evaluating the strongly inhomogeneous field near the cylinder. The resulting equation for the polarization vector is of the form

$$P_{\alpha, \mathbf{l}}(\mathbf{r}) = -4\pi k_0^2 \frac{\alpha}{v_0} \theta(\mathbf{r} - \mathbf{l}) \int d\mathbf{r}' G_{\alpha\beta}(\mathbf{r} - \mathbf{r}') \sum_{\mathbf{l}' \neq \mathbf{l}} P_{\beta, \mathbf{l}'}(\mathbf{r}'). \quad (18)$$

Next, we add to both sides of Eq. (18) a term

$$-4\pi k_0^2 \frac{\alpha}{v_0} \theta(\mathbf{r} - \mathbf{l}) \int d\mathbf{r}' G_{\alpha\beta}(\mathbf{r} - \mathbf{r}') P_{\beta, \mathbf{l}}(\mathbf{r}'), \quad (19)$$

which in fact corresponds to a local field correction. With this term included, the right-hand side of equation (18) can be evaluated using the Fourier transform of the scalar Green's function (14). In evaluating the left-hand side we take into account the δ -functional singularity of Green's function. As a result we obtain

$$(1 - 2\pi k_0^2 \frac{\alpha_{\perp}}{v_0} f) P_{l\alpha}(\mathbf{r}) = -4\pi \frac{\alpha_{\perp}}{v_0} f \theta(\mathbf{r} - \mathbf{l}) \int d\mathbf{r}' G_{\alpha,\beta}(\mathbf{r} - \mathbf{r}') \sum_{l'} P_{l'\beta}(\mathbf{r}) . \quad (20)$$

Performing the integral, we transform Eq. (20) into a dispersion equation for the TE waves:

$$(1 - 2\pi \frac{\alpha_{\perp}}{v_0} f) \delta_{\alpha\beta} = 4\pi k_0^2 \frac{\alpha_{\perp}}{v_0} f \sum_{\mathbf{G}} \frac{\theta^*(\mathbf{G})\theta(\mathbf{G} + \mathbf{q})}{\theta(\mathbf{q})[(\mathbf{q} + \mathbf{G})^2 - k_0^2]} \left[\delta_{\alpha\beta} - \frac{(\mathbf{q} + \mathbf{G})_{\alpha}(\mathbf{q} + \mathbf{G})_{\beta}}{k_0^2} \right] . \quad (21)$$

In the low-frequency region the main contribution to the sum in the right-hand side comes from the term with $\mathbf{G} = 0$. Neglecting other terms, we find

$$\epsilon_b k_0^2 = q^2 \left(\frac{1 - 2\pi\alpha_{\perp}/v_0 f}{1 + 2\pi\alpha_{\perp}/v_0 f} \right) , \quad (22)$$

which is the dispersion relation for TE waves in the Maxwell Garnett approximation. Taking into account terms with $\mathbf{G} \neq 0$ we can calculate the spectrum of lowest TE waves up to the boundary of the Brillouin zone by using the degenerate perturbation theory in the same way as we did it above for the TM waves. The corresponding perturbation series converges rapidly, but near the symmetry points it is again important to include degeneracy to first order by using correct zeroth-order linear combinations. For example, in a square lattice near the X point boundary the frequency is close to

$$k_{\perp} = \frac{G}{2\sqrt{\epsilon_{\perp} \pm \epsilon_{\perp}(G)}}, \quad \epsilon_{\perp}(G) = \frac{2f(\epsilon_{in} - \epsilon_{out})}{\epsilon_{in} + \epsilon_{out} + f(\epsilon_{in} - \epsilon_{out})} \frac{2J_1(GR)}{GR}, \quad G = \frac{2\pi}{a} . \quad (23)$$

This is again within $\pm 3\%$ from the exact result for a wide range of the filling factors and different permittivity ratios, cf. Fig. 4.

For both the TE and TM waves the zero-order in \mathbf{G} approximation (in which Bragg reflections are fully ignored) is not sensitive to the PC crystal structure and thus it is quantitatively equivalent to the homogeneous effective medium approximation. The only difference is that in a truly periodic structure there are no scattering losses from index fluctuations.

4. INHOMOGENEOUS SLAB IN THE WEAK GUIDING LIMIT

In this section we consider the weak waveguiding by an arbitrary thin inhomogeneous slab. We place no restriction on the degree of the inhomogeneity; what is important is the weak guiding power, $g \ll \lambda$. We shall consider periodic arrays of period a (PC slabs) in the instance of a planar arrangement of spherical particles, cylindrical rods, or cylindrical pores (see Figs. 1c,d). Periodicity of the arrangement is important even in the long wavelength limit $a \ll \lambda$ (since for an amorphous arrangement the Rayleigh scattering will be strong, as discussed in the next section). For periodic structures, our treatment applies all the way to the Brillouin zone boundary, as demonstrated in Sect. 3.

In all cases, we denote the dielectric permittivity of the guiding material by ϵ_g and that of the background by ϵ_b . The phase

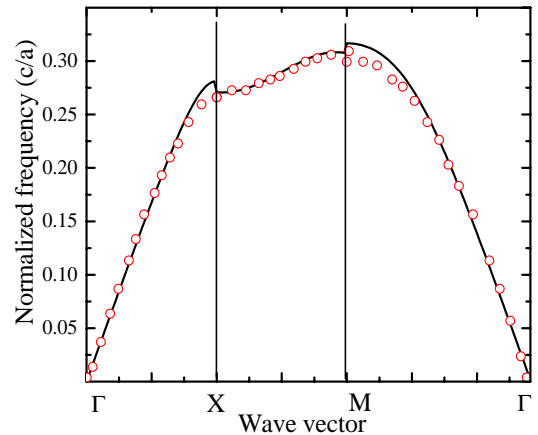


Figure 4. Low frequency spectra (TE polarization) of a photonic crystal (square lattice of cylindrical rods) calculated by the degenerate-state perturbation theory (solid lines). Point correspond to numerical calculation.⁴ The filling factor is $f = 0.1$ and $\epsilon_{in} = 11.96$; $\epsilon_{out} = 1$. In the interval XM the spectra are calculated more accurately, using more symmetry partners than for ΓX and ΓM intervals, hence the small discontinuities evident in the spectra at X and M points.

velocity of the wave guided by the slab can be obtained by a perturbative approach similar to that employed in the calculation of PC spectra in Section 3. In this approach we solve the wave equation by ignoring Bragg reflections in the zeroth approximation. Then we can include them by using perturbation theory with correct linear combinations of the zeroth-order waves.

In the long wavelength limit, the field inhomogeneity is important only at short distances away from the slab, since the short-range components of the fields decay exponentially over the distances of the order of a out of the slab. This allows us to identify TE-like and TM-like polarized waves and consider them separately.

For the TE-wave (electric field in the plane of inclusions) we start from the wave equation for the electric field \mathbf{E} in the form (7). For the wave propagating along x axis we seek the solution in the form $\mathbf{E}(\mathbf{r}) = \mathbf{E}_{\mathbf{q}} \exp(i\mathbf{q}\mathbf{r})$, with the propagation vector $\mathbf{q} \parallel x$. The boundary conditions of continuous tangential field imply for this geometry that in the long wavelength limit $qa \ll 1$ the dominant field component E_y is a smoothly varying function of the coordinates even within the thin slab.

Therefore, the evaluation of the wave phase velocity can be done in a way similar to the well-known solution of Schrödinger's equation for weakly confined states.²⁴ This analogy to the quantum mechanical problem of a particle bound to a one-dimensional potential well of small depth constitutes the central point for our analysis. In the Appendix we further illustrate its validity by considering an exemplary waveguide composed of homogeneous multiple layers with an arbitrary index profile.

Outside the slab, the dominant field component E_y satisfies a wave equation of the form

$$\frac{d^2}{dz^2} E_y + (k_b^2 - q^2) E_y = 0, \quad (24)$$

where \mathbf{q} is a 2D propagation vector and k_b is the frequency parameter normalized to the speed of light in the background material,

$$k_b^2 \equiv \epsilon_b k_0^2, \quad k_0 \equiv \omega/c. \quad (25)$$

In the transverse direction the field varies as $E_y = E_y(0) \exp -\kappa|z|$ with $\kappa = \sqrt{q^2 - k_b^2}$. Using Maxwell's equation $\text{div}\mathbf{D} = 0$, we can put the wave equation within the thin slab into the form

$$\Delta E_y + k_b^2 E_y = -4\pi k_0^2 \left(P_y + \nabla_y \sum_i \nabla_i P_i \right). \quad (26)$$

To obtain an additional relationship between κ and q we integrate Eq. (26) in the xy plane over the unit cell and in the z direction between points $\pm z_1$, such that $h \ll z_1 \ll 1/\kappa$. In the left-hand side the main contribution to this integral comes from the term $\partial^2 E_y / \partial z^2$ and distances remote from the plane, since the contribution of the second term is smaller by a factor κz_1 . Thus, the integral in the left-hand side reduces to $2\kappa E_y(0)$. In the right-hand side of Eq. (26) the main contribution to the integral comes from the inclusions themselves. For a highly inhomogeneous structure comprising spheres or cylindrical rods, this integral reduces (see below) to the y -component of the electric dipole moment of the unit cell, $P_y = \alpha E_y$, where α is the polarizability of the inclusion in the acting field of the wave and other inclusions. For a sphere, the polarizability is isotropic, $\alpha = R^3 \epsilon_b (\epsilon_g - \epsilon_b) / (\epsilon_g + 2\epsilon_b)$, while for cylinders the polarizability is highly anisotropic. For sufficiently elongated cylinders, $h/R \geq 10$, the transverse polarizability equals $\alpha_{\perp} = (1/2)R^2 h \epsilon_b (\epsilon_g - \epsilon_b) / (\epsilon_g + \epsilon_b)$.

The difference between the local field E_y and the average \overline{E}_y field outside the slab can be taken into account by adding the field contribution of the neighboring inclusions. For a square lattice the relation between the local and the average field is given by

$$E_y = \overline{E}_y + S^* \alpha n_s^{3/2} E_y, \quad (27)$$

where $n_s = a^{-2}$ and $S^* = 0.5 \sum' (n^2 + m^2)^{-3/2}$. The main contribution to the local field comes from nearest neighbors and is of the order of $R^3 n_s^{3/2}$. In contrast to the 3D case, the 2D lattice sum rapidly converges, giving $S^* \approx 4.41$. Equation (27) is obtained in the dipole approximation for the field of individual particles, and is strictly valid for $n_s R^2 \ll 1$.

For TE waves propagating along the plane of spheres or cylinders, the integration of the second term in the right-hand side of (26) can be transformed to an integration over the surface where $\mathbf{P} = 0$, so that the second term can be neglected. Integration of the first term gives the total polarization vector $P_y n_s$ per unit area of all inclusions in the average field E_y . Finally, for a square lattice of inclusions, we obtain

$$g_{\text{TE}} = 4\pi\alpha n_s \left(1 - S^* \alpha n_s^{3/2}\right)^{-1}. \quad (28)$$

When the local field corrections are negligible (low density of inclusions or small index contrast), then the guiding power can be expressed in terms of the average polarizability per unit area:

$$g_{\text{TE}} = \frac{4\pi}{s\epsilon_b} \int \alpha(\mathbf{r}) ds. \quad (29)$$

Comparing Eq. (29) for a monolayer of spheres of radius R with a homogeneous slab (Eq. 3) of thickness $2R$, we see that the guiding power of spheres is reduced by a factor $n_s R^2 \ll 1$, which is proportional to the filling factor of the guiding layer (volume fraction occupied by the spheres). This factor is responsible for the weak waveguiding. It is important, however, that the guiding remains in effect for arbitrary values of $n_s R^2$ and index contrast. The guiding power increases monotonically with the increasing filling factor and approaches the homogeneous layer value for $f \rightarrow 1$. Of course, before this limit is reached, local field effects will bring about special features, especially when the spheres begin to overlap.¹⁹

The waveguiding of TM waves is somewhat more complicated, since the localized magnetic field creates an inhomogeneous electric field across the layer. This makes difficult a direct use of the above procedure. However, according to Maxwell's equation, the displacement vector component D_z in a propagating wave is directly proportional to the magnetic field component H_y . Therefore, for weak confinement both H_y and D_z have a smooth spatial variation. This enables a modified procedure with the same idea as above (see also Appendix).

First, we rewrite the wave equation in terms of the displacement vector \mathbf{D} :

$$\Delta \mathbf{D} + k_b^2 \mathbf{D} = -4\pi(\Delta - \text{grad div})\mathbf{P}. \quad (30)$$

In the right-hand side of Eq. (30) the second derivatives $\partial^2 P_z / \partial z^2$ cancel, whereas the in-plane derivative $\partial^2 P_z / \partial x^2$ will produce a multiplier q^2 when averaged over the unit cell area. We can now seek the solution of Eq. (30) in the form $D_z = D_z(0) \exp(-\kappa|z|)$ with $\kappa = \sqrt{q^2 - k_b^2}$. We have

$$\frac{d^2}{dz^2} D_z + (k_b^2 - q^2) D_z = -4\pi q^2 P_z - 4\pi i q \frac{d}{dz} P_x. \quad (31)$$

Integrating Eq. (31) in the z direction between points $\pm z_1$, such that $h \ll z_1 \ll 1/\kappa$, and in the xy plane over the unit cell, we find a relationship similar to Eq. (1) from which we find both the spectrum and the guiding power for the TM mode. When integrating the right-hand side we note again that the second term does not contribute. The first term gives rise to a local field correction.

For a monolayer of spheres, the local field correction for the TM mode has the opposite sign and is twice larger than that for the TE mode. We find

$$g_{\text{TM}} = 4\pi\alpha n_s (1 + 2S^* \alpha n_s^{3/2})^{-1}. \quad (32)$$

Comparing Eq. (32) with Eq. (28) we see that the difference in the weak waveguiding by a plane of spheres is only due to the difference in the local field effects for different polarizations, since the polarizability of a single sphere does not depend on the polarization of the external field. When the local field effects are small ($n_s R^2 \ll 1$) the difference between polarizations disappears, in contrast to the case of a homogeneous layer.

In both cases the layer guiding power is determined by two factors: the individual polarizability of the higher-index inclusion, which is proportional to $(\epsilon_g - \epsilon_b)$, and the filling factor of the layer, $n_s R^2$.

The results above are equally valid for waves confined to an array of inclusions other than spheres, e.g. cylinders. However, one must use the appropriate value for the polarizability. For sufficiently elongated cylinders, $h/R \geq 10$, the parallel polarizability (appropriate for the TM-like mode) equals $\alpha_{\parallel} = (\epsilon_g - \epsilon_b)R^2h$. For a large index contrast, the guiding power for the TM mode substantially exceeds that for the TE mode.

For highly anisotropic cylinders, $h \gg R$, the guiding power of a slab composed of cylindrical rods varies strongly with the filling factor. For $f \ll 1$ we have $h/a \ll 1$ and g is controlled by the polarization of individual non-interacting cylinders. In this limit, the transverse polarizability is small and so is g_{TE} , whereas the longitudinal polarization of the slab and hence g_{TM} both increase due to the enhanced electric field between the cylinders. In contrast, for $h/a \gg 1$ the guiding power is in the regime of Maxwell-Garnett's effective permittivity, where the dipolar interaction between cylinders leads to strong local field effects. For these limiting cases the guiding powers are given by :

MG	cylinders	
$g_{TM} = hf(\epsilon_g - \epsilon_b)/[\epsilon_b + f(\epsilon_g - \epsilon_b)]$	$g_{TM} = hf(\epsilon_g - \epsilon_b)/\epsilon_b$	(33)
$g_{TE} = 2hf(\epsilon_g - \epsilon_b)/[\epsilon_g + \epsilon_b - f(\epsilon_g - \epsilon_b)]$	$g_{TE} = 2hf(\epsilon_g - \epsilon_b)/(\epsilon_g + \epsilon_b)$	

For $\epsilon_g \gg \epsilon_b$ the effective polarizability of the cylinder array for the TM mode grows at low f with the filling factor, but at a sufficiently large f it is strongly weakened by the local field effects. Therefore, at fixed h/R the dependence $g_{TM}(f)$ has a maximum. We find a nearly paradoxical conclusion that a film composed of cylinders or comprising pores can have a higher g_{TM} than that of a homogeneous high-permittivity film made of the same material and having the same thickness h .

For the TE mode the variation of g_{TE} with the h/a ratio is in the opposite direction, since the average transverse polarizability in the Maxwell Garnett regime is larger than the transverse polarizability of an individual cylinder. Thus the TM mode in a material with cylindrical pores or rods, such that $a > h > R$, should as a rule be much better confined than the TE mode.

Our results for the PC slab are in good agreement with numerical calculations. As an example, we show in Fig. 5 the spectra analytically calculated for an array of cylindrical rods (Fig. 1d) without including Bragg reflections. The entire spectra are described by one parameter g for each mode. The values of g (measured in units a/π) are $g_{TE} = 1.1$ and $g_{TM} = 3.2$. The weak waveguiding condition $g \ll \lambda$ is well fulfilled for both TE-like and TM-like guided waves in the low-frequency part of the spectrum. In this example the separation between cylinders ($h/a = 2$) is relatively small and the Maxwell Garnett approximation is found to work pretty well for both TE and TM modes. The calculated MG values are $g_{TE} = 1.5$ and $g_{TM} = 3.6$, while for separate cylinders one would have $g_{TE} = 1.3$ and $g_{TM} = 8.7$.

Results of the full-scale numerical calculation²⁵ are also shown in Fig. 5 by dots. The agreement is reasonably good, except near the Brillouin zone boundary.

Finally, we note that Eqs. (28, 32) also describe qualitatively the guiding power of an array of metallic inclusions.

Even though the permittivity of a metal at optical frequencies is negative, the predicted guiding power is positive. This means that waveguiding is in effect in this case too. To obtain a quantitative description, however, we must modify Eqs. (28, 32) to allow for the skin-effect and the damping of waves in the metallic particles.¹⁹

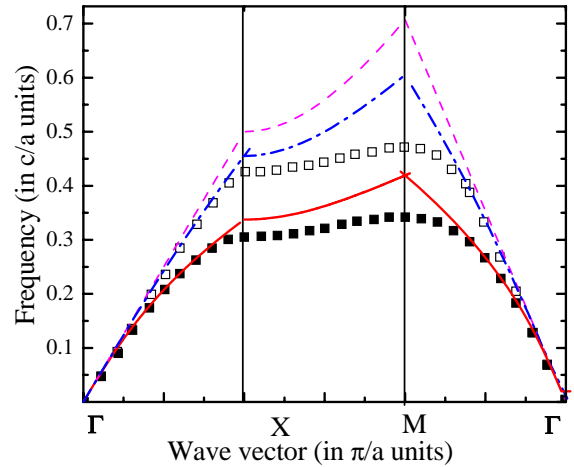


Figure 5. Low-frequency spectra of a photonic crystal slab composed of a square lattice of cylindrical rods calculated in the “guiding power” approximation Eq. 2 (solid lines: TM-like mode, dash-dotted lines: TE-like mode). The normalized guiding power values are: $g_{TM}=3.2$, $g_{TE}=1.1$. Results of the fill-scale numerical calculation²⁵ are shown by closed and open squares for the TM-like and TE-like modes, respectively; dashed line shows the edges of the light cone. The filling factor is $f = 0.125$ and the cylinder's permittivity is $\epsilon_{in} = 12$ with $\epsilon_{out} = 1$.

5. SCATTERING EXTINCTION OF LIGHT PROPAGATING IN A PC SLAB

Recently, a Brown University group²⁶ demonstrated the laser action in a uniaxially patterned silicon-on-insulator nanostructure. One of the surprising features of this remarkable accomplishment was the predominantly TM polarization of stimulated emission.²⁷ In our earlier work,¹² we carefully analyzed the photonics of this experiment and concluded that the TE mode was much better confined. Barring some exceptional anisotropy in the modal gain in the experiment²⁶ or some new and efficient mode-selective feedback mechanism, the TE mode should be winning in the competition to the lasing threshold.

However, it was recently noted that the structural variations in all state-of-the-art photonic crystal slabs are at least 2 to 7 % of the lattice spacings.²⁸ For example, the Brown group noticed conic variations of their nominally cylindrical pore shape.²⁷ We must therefore consider the radiation loss by the slab due to the scattering by unavoidable imperfections of the structure.

This type of radiation loss can be treated as Rayleigh-like scattering, modified by the local field redistribution in the patterned layer. For TE modes the radiation losses due to Rayleigh scattering from a PC slab were analyzed by Benisty et al.²⁹ and Koenderink et al.²⁸ in a strong waveguiding regime. The polarization dependence was not analyzed. In the weak waveguiding regime, however, this dependence is very important.

The difference arises for several reasons. *Firstly*, the boundary conditions on the propagating radiation (continuity of the tangential component of the electric field and the normal component of the displacement vector) lead to very different radiation losses for the TM and TE modes, especially for thin waveguiding structures with a large index contrast between the slab and the cladding regions.

This difference can be most easily evaluated using the reciprocity theorem for the emission: the field component i at a point A outside the slab generated by a unit dipole source, located at point B in the slab and oriented along the j axis, equals the j -th component of the field at point B generated by a unit dipole source located at point A and oriented along the i axis. Since the normal component of the field in the slab is $(\epsilon_{out}/\epsilon_{in})$ times weaker than outside, the same reduction of the field takes place when the light is emitted from a source inside the slab.

The tangential component of electric field is not reduced in a thin-layer waveguide, and so the overall ratio of the emission intensity from a dipole source normal to the layer to that from an in-plane dipole is $(\epsilon_{out}/\epsilon_{in})^2$. This ratio can be small in structures with a high contrast index. It can be also quite small for an asymmetric structure with different claddings. For a patterned Si slab on a SiO₂ substrate, the emission efficiency into air is ϵ_{Si}^2 times smaller for dipole sources normal to the plane. For emission into substrate it is reduced by a factor $\epsilon_{SiO_2}^2/\epsilon_{Si}^2$, so that the overall reduction is about a factor of 50.

Secondly, the lower confinement factor Γ for the TM mode is itself beneficial against the scattering loss from imperfections located in the core. Their effect is directly proportional to Γ .

Finally, the Rayleigh scattering mechanism (i.e. elastic scattering of the guided photon by the fluctuations of permittivity) depends on the spatial scale of the imperfections. When the imperfections are short-range, corresponding to variations of the size or position of individual inclusions, then the characteristic momentum transfer is large (of the order of the reciprocal inclusion size). In this situation, the mode separation from the light cone (see Fig. 6) is smaller for both modes than the typical momentum transfer. Therefore, the better confinement of the TE mode is not a defense against the radiation loss.

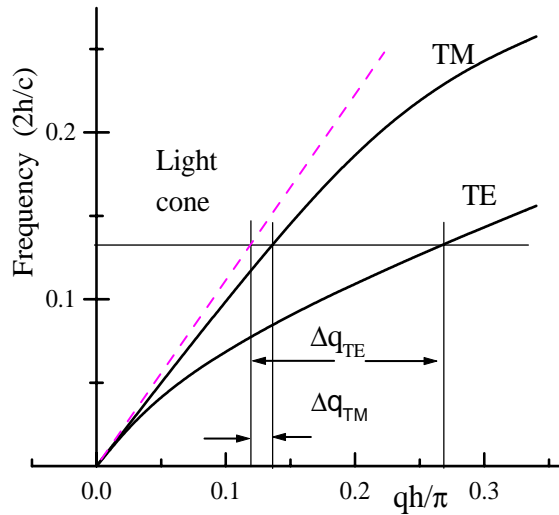


Figure 6. Momentum transfer in Rayleigh scattering of the guided mode from a patterned slab. Shown are the separations from the light cone for the two modes. This separation is proportional to squared guiding power of the mode.

The above considerations can be expressed quantitatively in terms of the Rayleigh scattering extinction coefficient η (defined as the inverse photonic mean free path).²³ For the case of weak confinement of TE waves by a guiding layer with cylindrical pores, the extinction coefficient can be written in the form

$$\eta_{\text{TE}} = \frac{2}{3\lambda^4} \Gamma \epsilon_{\text{out}}^2 \left(\frac{\epsilon_{\text{in}} - \epsilon_{\text{out}}}{\epsilon_{\text{in}} + \epsilon_{\text{out}}} \right)^2 v_0 f \langle \delta^2 \rangle, \quad (34)$$

where $v_0 = \pi R^2 h$ is the volume of one cylinder, Γ is the modal confinement factor, and $\langle \delta^2 \rangle$ is a reciprocal fluctuation parameter. For the parameters of the experiment²⁶ this gives $\eta_{\text{TE}} \approx 5 \langle \delta^2 \rangle \text{cm}^{-1}$. For a random distribution of cylinders, when the individual scattering processes can be considered independent, one has $\langle \delta^2 \rangle = 1$. For a model, in which the cylinder radius is the fluctuation parameter, one has $\langle \delta^2 \rangle = 4 \langle (\delta r)^2 \rangle / \langle r \rangle^2$.

For the TM waves, expression (34) must be multiplied by the factor $(\epsilon_{\text{out}}/\epsilon_{\text{in}})^2$. Besides this factor, the resultant η_{TM} is also reduced by the smaller Γ for TM waves.

6. CONCLUSION

We have considered the polarization-dependent waveguiding of light by thin highly inhomogeneous slabs embedded in a uniform medium. We examined exemplary slab structures comprising a monolayer of periodically patterned dielectric spheres, cylinders, or cylindrical pores etched in a dielectric medium. We also discussed 2D photonic crystals (PC) corresponding to a periodic arrangement of infinitely long cylinders. Because of the uniaxial nature of the pattern, the propagation of waves in the direction perpendicular to the axis depends on the polarization and we considered separately the TE and TM polarized waves.

We have demonstrated an effective approach to calculating the low-frequency part of the spectra of patterned periodic structures. In this approach we ignore to zeroth-order the Bragg scattering by crystalline planes but include local field effects in first order perturbation theory. This results in an effective medium approximation, similar to Maxwell-Garnett's theory but with modified local field corrections. Perturbation approach converges rapidly for both 2D photonic crystals and thin periodically patterned slabs. The Bragg reflections are shown to be important only near points of symmetry-induced spectral degeneracy, where they can be taken into account by the degenerate perturbation theory, using correct linear combination of a small number of zero-order waves. The resultant analytically evaluated spectra are compared with available numerical computations. Excellent agreement is found for the low-frequency spectra all the way to the Brillouin zone boundary.

Apart from the Bragg splittings, the spectra are well described by a single frequency-independent parameter g , which we call the guiding power. Simple analytic formulae are presented for g for both TM and TE polarizations. Comparing these formulae with similar expressions for slabs of same thickness h but composed of homogeneous uniaxial media, we derive the principal values of the effective homogeneous permittivity that provides identical waveguiding. While it is intuitively "obvious" that in the long wavelength limit the existence of guided waves relies on some average index profile, the exact nature of this averaging is elucidated for the first time.

Regularity of the periodic pattern is important for our analysis because it allows us to consider the waveguiding without taking into account the Rayleigh-like scattering of waves by imperfections. So long as scattering is negligible, our results for the guiding power are applicable to "amorphous" arrangements of same density. The criterion for weak scattering by amorphous arrangements is $h \gg a$, where a is the typical distance between inclusions. However, scattering by imperfections is usually not negligible even when the structures are nominally designed to be periodic. This leads to an extinction of guided waves via the radiation scattered out of the slab. For a high index contrast, the extinction coefficient depends strongly on the polarization and favors the TM wave. The TE waves that are normally better confined are scattered out more efficiently, in part because of the higher scattering probability and in part because the better confinement leads to higher exposure of TE waves to lattice imperfections in the slab.

ACKNOWLEDGMENTS

This work was supported by the NY State Center for Advanced Sensor Technology (Sensor CAT) at Stony Brook.

REFERENCES

1. E. Yablonovitch, T. J. Gmitter and K. M. Leung, "Photonic band structure: The face-centered-cubic case employing nonspherical atoms," *Phys. Rev. Lett.* **67**, pp. 2295-2298, 1991.
2. O. Painter, R. K. Lee, A. Scherer, A. Yariv, J. D. O'Brien, P. D. Dapkus, and I. Kim "Two-dimensional photonic band-gap defect mode laser," *Science* **284**, pp. 1819-1821, 1999.
3. J. D. Joannopoulos, R. D. Meade and J. N. Winn, *Photonic Crystals: Molding the Flow of Light*, Princeton University, Princeton, NJ, 1995.
4. M. Plihal and A. A. Maradudin, "Photonic band structure of two-dimensional systems: The triangular lattice," *Phys. Rev.* **B 44**, pp. 8565-8571, 1991; V. Kuzmyak, A. A. Maradudin and A. R. McGurn, "Photonic band structure of two-dimensional systems fabricated from rods of a cubic polar crystal," *ibid.* **B 55**, pp. 4298-4311, 1997.
5. N. A. Nicorovici, R. C. McPhedran and L. C. Botten, "Photonic band gaps for arrays of perfectly conducting cylinders," *Phys. Rev.*, **E 52**, pp. 1135-1145, 1995.
6. K. Ohtaka, T. Ueta and K. Amemiya, "Calculation of photonic bands using vector cylindrical waves and reflectivity of light for an array of dielectric rods," *Phys. Rev.* **B 57**, pp. 2550-2568, 1998.
7. A. Taflove, *Computational Electrodynamics - The Finite-Difference Time-Domain Method*, Artech House, Boston, MA, 1995.
8. M. Boroditsky, R. Coccioli and E. Yablonovitch, "Analysis of photonic crystals for light emitting diodes using the finite difference time domain technique," *Photonics West*, 1998.
9. A. K. Sarychev and V. M. Shalaev, "Electromagnetic field fluctuations and optical nonlinearities in metal-dielectric composites," *Physics Reports* **335**, pp. 275-371, 2000.
10. A. A. Krokhin, P. Halevi and J. Arriaga, "Long-wavelength limit (homogenization) for two-dimensional photonic crystals," *Physical Review* **B 65**, 115208-17, 2002.
11. N. A. Nicorovici, R. C. McPhedran and L. C. Botten, "Photonic band gaps: noncommuting limits and the "acoustic band," *Phys. Rev. Letters* **75**, pp. 1507-1520, 1995.
12. A. V. Subashiev and S. Luryi, "Modal control in semiconductor optical waveguides with uniaxially patterned layers," *IEEE J. Lightwave Technology* **24**, issue 3, 2006 (in print).
13. D. Marcuse, *Theory of Dielectric Optical Waveguides*, Academic Press, Boston, 1991.
14. M. J. Adams, *An Introduction to Optical Waveguides*, Wiley, New York, 1981.
15. T. D. Visser, H. Blok, B. Demeulenaere, and D. Lenstra, "Confinement factors and gain in optical amplifiers," *IEEE J. Quant Electron.* **33**, pp. 1763-766, 1997.
16. Y-Z. Huang, Z. Pan and R-H. Wu, "Analysis of optical confinement in semiconductor lasers," *J. Appl. Phys.* **79**, pp. 3827-3830, 1996.
17. T. Ochiai and K. Sakoda, "Nearly free-photon approximation for two-dimensional photonic crystal slab", *Phys. Rev.* **B64**, pp. 045108-11, 2001.
18. J. Vuckovic, M. Loncar, H. Mabuchi, and A. Scherer, "Optimization of Q-factor in photonic crystal microcavities," *IEEE Journal of Quantum Electronics* **38**, pp. 850-856, 2002.
19. A. K. Sarychev and V. M. Shalaev, "Electromagnetic field fluctuations and optical nonlinearities in metal-dielectric composites," *Physics Reports* **335**, pp. 275-371, 2000.
20. A. L. Efros and A. L. Pokrovsky, "Dielectric photonic crystal as media with negative electric permittivity and magnetic permeability," *Sol. State Comm.* **129**, pp.643-647, 2004.
21. E.L. Ivchenko, *Superlattices And Other Heterostructures: Symmetry And Optical Phenomena*, Springer-Verlag, Berlin and Heidelberg, 1997.
22. L. D. Landau, E. M. Lifshits and L. P. Pitaevskii, *Statistical physics*, Pergamon Press, Oxford, New York, 1980; Course of theoretical physics v 5,9 ; Vol. 2 by E.M. Lifshitz and L.P. Pitaevskii.
23. L.D. Landau and E.M. Lifshitz, *Electrodynamics of Continuous Media*, Pergamon Press, Oxford, 1960.
24. L.D. Landau and E.M. Lifshitz, *Quantum Mechanics: Non-Relativistic Theory*, Pergamon Press, Oxford, 1977.
25. S. Johnson, P. R. Villeneuve, S. Fan, and J. D. Joannopoulos, "Linear waveguides in photonic-crystal slabs", *Physical Review* **B 62**, pp. 8212-8222, 2000.

26. S. G. Cloutier, P. A. Kosyrev and J. M. Xu, "Optical gain and stimulated emission in periodic nanopatterned crystalline silicon," *Nature Materials* **4**, 887-891, 2005.
27. J. M. Xu, private communication
28. A. F. Koenderink, A. Lagendijk, and W. L. Vos, "Optical extinction due to intrinsic structural variations of photonic crystals," *Physical Review B* **72**, pp. 153102-1-4, 2005.
29. H. Benisty, D. Labilloy, C. Weisbuch, C. J. M. Smith, T. F. Krauss, D. Cassagne, A. Beraud, and C. Jouanin, "Radiation losses of waveguide-based two-dimensional photonic crystals: Positive role of the substrate," *Applied Physics Letters* **76**, pp. 532-534, 2000.

Appendix. Guiding power of a homogeneous layer with arbitrary index profile

Let the index profile depend only on z and the wave propagation be in x direction. First consider the case of a TM mode, which has more complicated boundary conditions and electric field distribution. We shall analyze this case using two equivalent approaches. In the first approach we divide the guiding region where $\epsilon(z) \neq \epsilon_b$ into N sublayers and match the solutions with appropriate boundary conditions. This approach will give us an insight for the approximation implied in the "guiding power" approach.

For the TM mode there is only one non-zero component of the magnetic field, H_y , so that it is convenient to use the wave equation for $H_y = H_y(z) \exp(iqx)$ which is of the form¹⁴

$$\frac{d}{dz} \frac{1}{\epsilon(z)} \frac{d}{dz} H_y(z) - \frac{q^2}{\epsilon(z)} H_y(z) = k_0^2 H_y. \quad (\text{A.1})$$

Solutions of Eq. (A.1) in individual layers can be written as

$$\begin{aligned} H_0 &= a_0 \exp(\kappa z) & z \leq 0 \\ H_1 &= a_1 \sin(k_1 z + \phi_1) & 0 < z \leq h/N \\ \dots & \dots & \dots \\ H_i &= a_i \sin(k_i z + \phi_i) & h/n(i-1) < z \leq h/Ni \\ \dots & \dots & \dots \\ H_N &= a_N \exp(-\kappa z) & z \leq 0 \end{aligned} \quad (\text{A.2})$$

At each boundary the logarithmic derivatives $d/dz \ln[H_y(z)/\epsilon(z)]$ should be equal, whence we have

$$\begin{aligned} \kappa/\epsilon_b &= k_1 \text{ctn}(\phi_1)/\epsilon_1 \\ k_1 \text{ctn}(k_1 h/N + \phi_1)/\epsilon_1 &= k_2 \text{ctn}(\phi_2)/\epsilon_2 \\ \dots & \dots \\ k_i \text{ctn}(k_i h/N + \phi_i)/\epsilon_i &= k_{i+1} \text{ctn}(\phi_{i+1})/\epsilon_{i+1} \\ \dots & \dots \\ k_N \text{ctn}(k_N h/N + \phi_N)/\epsilon_N &= -\kappa/\epsilon_b \end{aligned} \quad (\text{A.3})$$

Here $\epsilon_i = [\epsilon(h/N)(i-1) + \epsilon(hi/N)]/2$ and $k_i = \sqrt{k_0^2 \epsilon_i - q^2}$. The system (A.3) can be simplified in the weak waveguiding limit, when κ is small. To be precise, we assume that $\text{ctn}(\phi_1) \approx (\kappa/k_1)(\epsilon_1/\epsilon_b) \ll 1$ and $\text{ctn}^2(\phi_i) \ll 1$ for all i . Then, for $N \gg 1$ we can approximate $k_i \text{ctn}(k_i h/N + \phi_i) \approx k_i \text{ctn}(\phi_i) + k_i^2 h/N$ and add all equations. In the limit $N \rightarrow \infty$ the sum is replaced by an integral, giving

$$2 \frac{\kappa}{\epsilon_b} = \int_0^h \left(k_0^2 - \frac{q^2}{\epsilon(z)} \right) dz, \quad (\text{A.4})$$

Taking in the zeroth-order approximation $q^2 = \epsilon_b k_0^2$, we obtain

$$\kappa = \frac{1}{2} k_b^2 \int_0^h \left(1 - \frac{\epsilon_b}{\epsilon(z)} \right) dz, \quad (\text{A.5})$$

The dispersion relation for the guiding wave reads $q = \sqrt{\epsilon_b k_0^2 + \kappa^2}$ which agrees with the well-known result for the standard three-layer waveguide.¹³

This result is used in our paper to study the waveguiding by layers with a periodic arrangement of inclusions in the propagation plane. For such geometries the equation for magnetic field becomes cumbersome because of the complicated boundary conditions. However, the normal component of the electric displacement vector D_z remains a smoothly varying function. Let us demonstrate that integration of the equation for \mathbf{D} leads to the same result for the guiding power as the above system of equations for a set of sublayers with proper boundary conditions.

The displacement vector $\mathbf{D} = \epsilon(z)\mathbf{E}$ can be written in the form

$$\mathbf{D} = \epsilon_b \mathbf{E} + \frac{\epsilon(z) - \epsilon_b}{\epsilon(z)} \mathbf{D}, \quad (\text{A.6})$$

whence the wave equation (30) becomes

$$\Delta \mathbf{D} - \text{grad div} \frac{\epsilon(z) - \epsilon_b}{\epsilon(z)} \mathbf{D} = -k_b^2 \mathbf{D}, \quad (\text{A.7})$$

The displacement vector has two non-zero components D_z, D_x . We will write down the equation for D_z , seeking it in the wave-like form $D_z = D_z(z) \exp(iqx)$, viz.

$$\frac{d^2}{dz^2} D_z(z) - (q^2 - k_b^2) D_z - q^2 \frac{\epsilon(z) - \epsilon_b}{\epsilon(z)} D_z + \frac{d^2}{dz dx} \left(\frac{\epsilon(z) - \epsilon_b}{\epsilon(z)} D_x(z) \right) = 0. \quad (\text{A.8})$$

Integrating Eq. (A.8) over z from $-z_1$ to z_1 , where z_1 is the distance at which the permittivity becomes equal to ϵ_b and no longer depends on z , we note that the term with D_x does not contribute. In the same approximation as above ($q^2 = \epsilon_b k_0^2$) we get

$$2\kappa = q^2 \int_{-\infty}^{\infty} \left(1 - \frac{\epsilon_b}{\epsilon(z)} \right) dz, \quad (\text{A.9})$$

which is equivalent to Eq. (A.5).

For the TE mode the electric field has only y component. The wave equation for the electric field $E_y = E_y(z) \exp(iqx)$ is of the form

$$\frac{d^2}{dz^2} E_y(z) = [q^2 - k_0^2 \epsilon(z)] E_y. \quad (\text{A.10})$$

We now integrate Eq. (A.10) between $-z_1$ and z_1 , that is over the region where the permittivity is variable. At $z \geq z_1$ the solution of the Eq. (A.10) has the form $E_y(z) = E(0) \exp(\pm \kappa z)$ and we get

$$-2\kappa E_y(0) = \int_{-z_1}^{z_1} (q^2 - k_0^2 \epsilon(z)) E_y(z) dz. \quad (\text{A.11})$$

In the limit of weak waveguiding, $\kappa z_1 \ll 1$ and $E_y(z)$ is a slowly varying function across the entire layer. Therefore it can be replaced in the integral by a constant value taken, e.g., at $z = 0$. Outside the guiding layer we have $q^2 = \epsilon_b k_0^2 + \kappa^2$ and hence in Eq. (A.11) we can take as the zeroth-order approximation $q^2 = \epsilon_b k_0^2$. Thus, we get

$$\kappa = \frac{1}{2} \epsilon_b k_0^2 \int_{-\infty}^{\infty} \left(\frac{\epsilon(z)}{\epsilon_b} - 1 \right) dz. \quad (\text{A.12})$$

We have replaced the limits of integration in Eq. (A.12) by $\pm\infty$ since the region where $\epsilon(z) = \epsilon_b$ does not contribute to the integral. The dispersion of the guiding wave is $q = \sqrt{\epsilon_b k_0^2 + \kappa^2}$.

Equations (A.5) and (A.12) can be rewritten in terms of the guiding power, cf. Eq. (4).